12

Coulomb Plus Nuclear Interactions

So far, we have discussed phase shift functions which increase or decrease monotonically with the impact parameter b. These are either short-range nuclear interactions whose magnitudes are falling off with b, or long-range Coulomb interactions, slowly increasing with b. In this chapter we will discuss combinations of such interactions. The first of these phase shift functions will be purely real. Again, some qualitatively new features appear.

With combinations of short-range and Coulomb interactions, the overall phase shift function can be written as

$$X(b_x) = X_{\mathrm{N}}(b_x) + X_{\mathrm{C}}(b_x), \tag{12.1}$$

where $X_{\mathrm{N}}(b_x)$ is some short-range nuclear interaction and the Coulomb part has the property that

$$X_{\mathrm{C}}(b_x) \to X_{\mathrm{pt}}(b_x) = -C_\infty + 2\eta \log b_x, \tag{12.2}$$

for b_x much larger than the Coulomb screening radius, and with C_∞ determined by details of the screening. For the Coulomb part, we shall throughout this chapter adopt the phase shift function Eq. (11.20) studied in Section 11.3 with $C_\infty = 0$,

$$X_{\mathrm{C}}(b_x) = 2\eta \log \sqrt{a^2 + b_x^2}. \tag{12.3}$$

Such combinations Eq. (12.1) of phase shift functions can lead to a rich variety of cross section patterns.

Because of the long tail of the Coulomb phase shift function, the exact numerical integral against which we want to compare the asymptotic approximation, needs to be evaluated with some care. This can be achieved by writing

$$\exp[iX(b_x)] = \exp[iX_{\mathrm{C}}(b_x)] + \{\exp[iX(b_x)] - \exp[iX_{\mathrm{C}}(b_x)]\}. \tag{12.4}$$

Downloaded from https://www.cambridge.org/core. UNIVERSIDAD AUTONOMA METROPOLITANA, on 16 Nov 2026 at 17:41:26, subject to the Cambridge Core terms of use, available at https://www.cambridge.org/core/terms. https://doi.org/10.1017/9781316219256.016

Then, the diffraction integral can be split as [see Eq. (7.29)]

$$\begin{aligned} F(q) &= -ik\int_0^\infty J_0(qb_x)\exp[iX(b_x)]b_x\,\mathrm{d}b_x \\ &= F_{\mathrm{C}}(q) - ik\int_0^\infty J_0(qb_x)\big\{\exp[iX(b_x)] - \exp[iX_{\mathrm{C}}(b_x)]\big\}b_x\,\mathrm{d}b_x \\ &= F_{\mathrm{C}}(q) + ik\int_0^\infty J_0(qb_x)\exp[iX_{\mathrm{C}}(b_x)]\big\{1 - \exp[iX_{\mathrm{N}}(b_x)]\big\}b_x\,\mathrm{d}b_x. \end{aligned} \tag{12.5}$$

In this last form, it is clear that the unspecified phase arising from screening remains an overall factor, common to both parts. For the Coulomb amplitude $F_{\mathrm{C}}(q)$ we take the form given in Section 11.3 with $C_\infty = 0$, corresponding to the phase shift function Eq. (12.3). The remaining term, involving the curly bracket in the last line of Eq. (12.5), is a convergent integral.

There is one other technical issue here. With a distributed charge like that represented by the phase shift function Eq. (12.3), the asymptotic approximation to the Coulomb amplitude $F_{\mathrm{C}}(q)$ that we extract will have a rainbow singularity at some momentum transfer $q_{\mathrm{R}}^{\mathrm{Coul}}$. This singularity is an artifact of the asymptotic approximation, there is no analogous singularity contained in the numerical integral against which it could cancel; the overall amplitude has no singularity at that value of the momentum transfer (but possibly at some other value).

12.1 Real Gaussian Plus Coulomb

We consider first the composite phase shift function

$$X(b_x) = A_{\mathrm{g}}\exp(-b_x^2/\beta^2) + 2\eta\log\sqrt{a^2 + b_x^2}. \tag{12.6}$$

As a reference, we shall keep the Coulomb part fixed, with $\eta > 0$, corresponding to repulsion. For the short-range nuclear part,

$$X_{\mathrm{N}}(b_x) = A_{\mathrm{g}}\exp(-b_x^2/\beta^2), \tag{12.7}$$

we shall consider both attraction ($A_{\mathrm{g}} > 0$) and repulsion ($A_{\mathrm{g}} < 0$).

For simple phase shift functions, including those that are real and fall off monotonically in magnitude as the impact parameter b increases, there is a simple relationship between the classical concepts of attraction and repulsion and the sign of the phase shift function, as discussed in Chapter 3. We recall that the force is related to the gradient of the potential, whereas the phase shift function is given by a line integral through the potential. For these simple phase shift functions, a

Downloaded from https://www.cambridge.org/core. UNIVERSIDAD AUTONOMA METROPOLITANA, on 16 Nov 2026 at 17:41:26, subject to the Cambridge Core terms of use , available at https://www.cambridge.org/core/terms. https://doi.org/10.1017/9781316219256.016

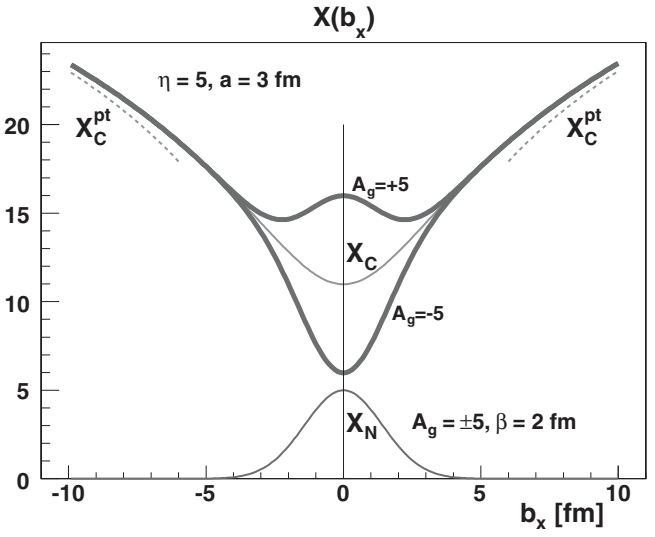


Figure 12.1 Phase shift functions $X_{\mathrm{C}}(b_x)$ and $X_{\mathrm{N}}(b_x)$, with X_{N} given as the Gaussian of Eq. (12.7), as well as their sum (for both signs of A_{g}). For comparison, also the point-Coulomb phase shift function is indicated at large $|b_x|$ as $X_{\mathrm{C}}^{\mathrm{pt}}$.

repulsive potential ($V(r) > 0$) leads to a negative phase shift function ($\chi(b) < 0$) whose derivative is positive ($X'(b_x) > 0$ for b_x real and positive). The Coulomb phase shift function is superficially in conflict with this correspondence, since we have subtracted the infinite, negative screening constant, C_∞.

For a representative set of parameters, we show the two parts of this phase shift function, as well as the sum (for both signs of A_{g}) in Fig. 12.1. The corresponding derivatives, which for a given momentum transfer q determine the points of stationary phase, are given in Fig. 12.2. Again, we display both the individual contributions and their sum (for both signs of A_{g}). Clearly, at small momentum transfers, the Coulomb part will dominate, with the main contribution coming from the far-out Coulomb stationary point, and the scattering cross section will be similar to those described in Section 11.3.

However, there will be additional contributions from one or more stationary points at shorter distances. We see from Fig. 12.2 that if the short-range interaction is repulsive, with $A_{\mathrm{g}} < 0$, there will be one additional stationary point, as was already the case for the distributed-charge phase shift function $\chi_1(b)$ studied in Section 11.3. But now the additional stationary point is occurring at a shorter distance than was the case for the pure Coulomb scattering, and the corresponding rainbow point will occur at a higher value of momentum transfer. For an attractive short-range interaction, however, there can at small momentum transfers be a total

Downloaded from https://www.cambridge.org/core. UNIVERSIDAD AUTONOMA METROPOLITANA, on 16 Nov 2026 at 17:41:26, subject to the Cambridge Core terms of use, available at https://www.cambridge.org/core/terms. https://doi.org/10.1017/9781316219256.016

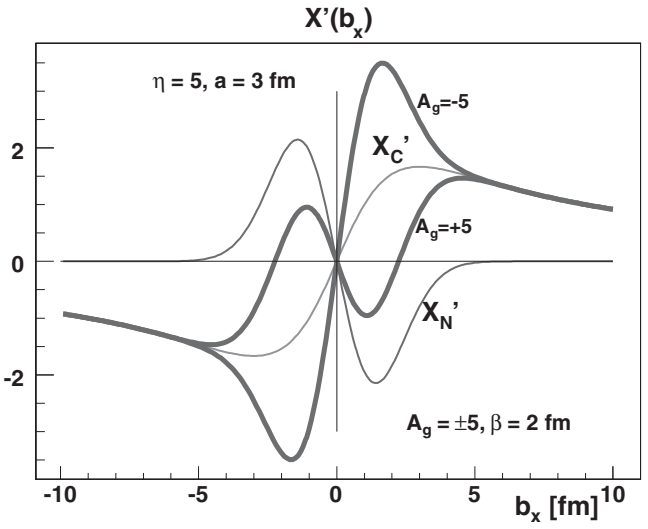


Figure 12.2 Derivatives of phase shift functions: $X'_{\mathrm{C}}(b_x)$ and $X'_{\mathrm{N}}(b_x)$, with X_{N} given as the Gaussian of Eq. (12.7), as well as their sum (for both signs of A_{g}).

of four points of stationary phase, as indeed is the case for the parameters adopted for Figs. 12.1 and 12.2. This will lead to *two* rainbow points! In contrast to the secondary rainbow observed in the scattering of light from water drops, here the two rainbows are quite independent of each other, occurring at rather different scattering angles. In fact, one rainbow is due to repulsion (positive $\mathrm{Re}\, b_x$), the other is due to attraction ($\mathrm{Re}\, b_x < 0$).

On the other hand, at large momentum transfers the short-range interaction will dominate, the points of stationary phase will occur off the real axis, giving a differential cross section reminiscent of those described for the real Gaussian phase shift function in Sections 7.1 and 7.3.

In analogy with Fig. 7.2, we show in Figs. 12.3 and 12.4 for the two cases $A_{\mathrm{g}} < 0$ and $A_{\mathrm{g}} > 0$, respectively, regions in the complex b_x-plane where $\mathrm{Re}\, X'(b_x)$ is positive (white) and where it is negative (shaded). Stationary points will be found where $\mathrm{Re}\, X'(b_x)$ is positive, and where simultaneously $\mathrm{Im}\, X'(b_x)$ vanishes (dashed lines superimposed on the figure, including in these cases the real axis). Also, where two such lines of vanishing $\mathrm{Im}\, X'(b_x)$ cross at 90° (in a white region), there will be a rainbow point.

When dealing with more complicated phase shift functions, such "maps" are very useful for easily identifying where possible stationary points can be found (along dashed lines in the white regions). They also reveal where rainbow points are to be found (where two dashed curves cross at an angle of 90°).

Downloaded from https://www.cambridge.org/core. UNIVERSIDAD AUTONOMA METROPOLITANA, on 16 Nov 2026 at 17:41:26, subject to the Cambridge Core terms of use, available at https://www.cambridge.org/core/terms. https://doi.org/10.1017/9781316219256.016

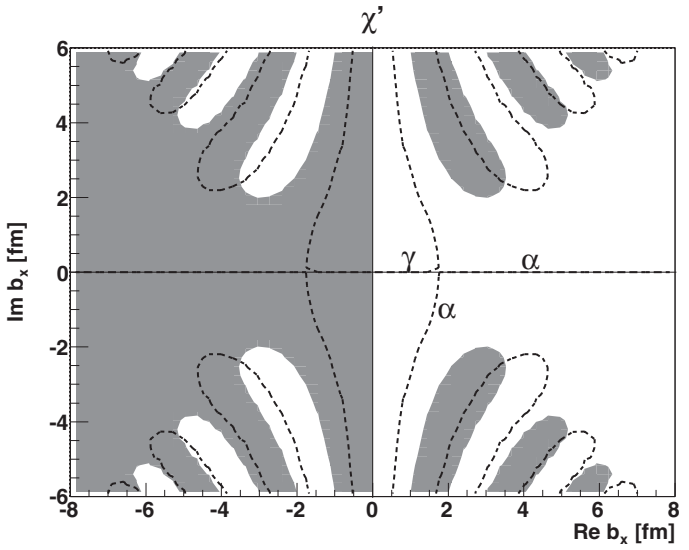


Figure 12.3 Regions of positive (white) and negative (shaded) values of $\mathrm{Re}\, X'(b_x)$, shown in the complex b_x-plane for $A_\mathrm{g} = -5$. The figure is analogous to Fig. 7.2, except that here $\beta = 2$ fm and that the phase-shift function now also has a Coulomb part. Also indicated as dashed lines, are the locations where $\mathrm{Im}\, X'(b_x) = 0$ (in this case, including the real axis). A rainbow point occurs at $b_x = 1.65$ fm.

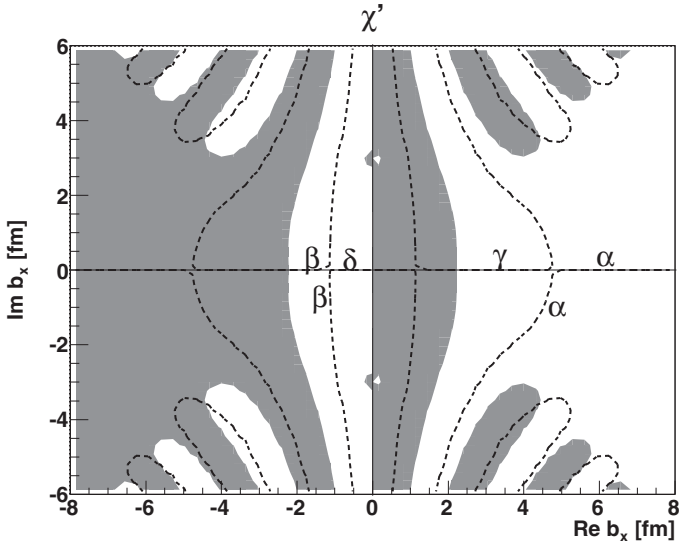


Figure 12.4 Analogous to Fig. 12.3 except that the short-range interaction is also attractive, $A_\mathrm{g} = +5$. Rainbow points occur for $b_{\mathrm{R}1} = -1.09$ fm and $b_{\mathrm{R}2} = 4.55$ fm.

Downloaded from https://www.cambridge.org/core. UNIVERSIDAD AUTONOMA METROPOLITANA, on 16 Nov 2026 at 17:41:26, subject to the Cambridge Core terms of use , available at https://www.cambridge.org/core/terms. https://doi.org/10.1017/9781316219256.016

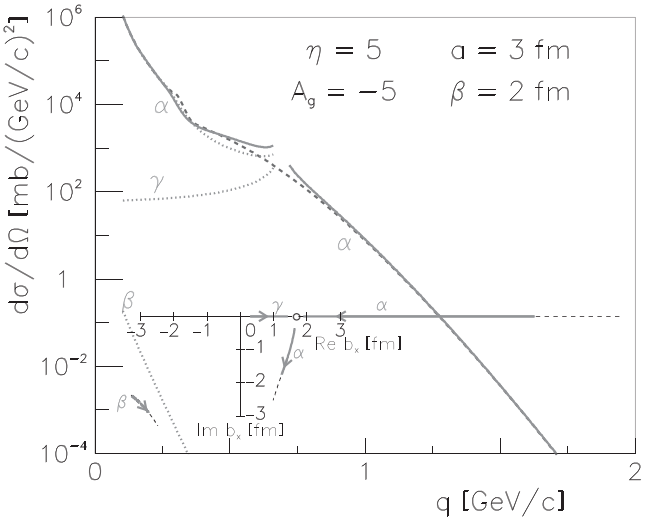


Figure 12.5 Differential cross section for the phase shift function Eq. (12.6). The inserts show the trajectories of stationary points for $0.16\ \text{GeV/c} \leq q \leq 6.0\ \text{GeV/c}$ (dotted). The parts that correspond to the cross section plots, $0.2\ \text{GeV/c} \leq q \leq 2.0\ \text{GeV/c}$ are shown as solid curves. The open circle represents the rainbow point. The cross sections contributed by the individual stationary points, α, β, and γ, are shown as dotted curves. The solid curves give the resulting interference pattern, with the gap around $q_{\text{R}} = 0.69\ \text{GeV/c}$ representing a rainbow singularity.

12.1.1 Repulsive Gaussian Plus Coulomb

We start by discussing the case of a repulsive short-range interaction. As is seen from Figs. 12.2 and 12.3, this is a somewhat simpler case than the mixed case, in the sense that there is only one rainbow.

In Fig. 12.5 we display the differential cross section corresponding to the combined phase shift function Eq. (12.6) for this case of short-range repulsion, $A_{\text{g}} = -5$. A forward Coulomb cross section (completely dominated by the contribution of the Coulomb stationary-phase point α) is followed by a transition region with a rainbow at somewhat larger momentum transfer than in the pure Coulomb case of Section 11.3, determined by the contributions of the stationary points α and γ. Then, at larger values of q, there is a smooth fall-off, similar to that seen in Fig. 7.3 for the real Gaussian phase-shift function. The contribution from the stationary point β is everywhere subdominant.

The agreement between the asymptotic approach and the numerical result (shown by the dashed curve) is again quite good, except for the region of the rainbow point ($q_{\text{R}} = 0.69\ \text{GeV/c}$), as well as the region of the Coulomb rainbow point ($q_{\text{R}}^{\text{Coul}} = 0.33\ \text{GeV/c}$), as discussed above. Immediately beyond the rainbow

Downloaded from https://www.cambridge.org/core. UNIVERSIDAD AUTONOMA METROPOLITANA, on 16 Nov 2026 at 17:41:26, subject to the Cambridge Core terms of use, available at https://www.cambridge.org/core/terms. https://doi.org/10.1017/9781316219256.016

point, the cross section is seen to fall more rapidly. This can be understood in terms of the stationary point α moving away from the real axis.

12.1.2 Attractive Gaussian Plus Coulomb

As was already evident from Fig. 12.2, when the short-range interaction is attractive ($A_g > 0$), the situation is more rich in structure, with the possibility of having two rainbow points. For the parameters chosen for that figure, there are indeed two rainbow points. Whether this phase shift function leads to one or two rainbows, is determined by whether or not $X'(b_x = 0)$ has a positive or negative slope at the origin. In fact, for the phase shift function Eq. (12.6), we have

$$X'(b_x) \to -2\frac{b_x}{\beta^2}A_g + 2\eta\frac{b_x}{a^2}, \quad \text{as } b_x \to 0. \tag{12.8}$$

With $\eta > 0$, we see that this slope becomes negative (see Fig. 12.2) for $A_g > 0$ (attraction) *and* provided

$$\eta < \left(\frac{a}{\beta}\right)^2 A_g, \tag{12.9}$$

which then, within this model, is the condition for having two rainbows. For the parameters adopted in Figs. 12.1, 12.2, and 12.4 these two rainbow points are located at $q_{R1} = 0.19$ GeV/c and $q_{R2} = 0.29$ GeV/c.

The resulting differential cross section is shown in Fig. 12.6. At low momentum transfers, the asymptotic approach has contributions from four points of stationary phase (see also Fig. 12.2). Two of these are at positive values of $\mathrm{Re}\, b_x$ (the far-out one is associated with the Coulomb repulsion), and two are at negative values. The latter are associated with the short-range attraction.

The two rainbow points, which are rather close to each other, make it natural to discuss separately three regions of momentum transfer. At low momentum transfers, inside the first rainbow (at $q_{R1} = 0.19$ GeV/c, corresponding to the nuclear attraction), the cross section is dominated by the outer Coulomb trajectory, denoted α. In fact, the other contributions, including those corresponding to the first rainbow, β and δ, are subdominant compared to the α-contribution. As a result, this first rainbow singularity is practically invisible.

Between the two rainbows, there are three contributions, from the stationary points denoted α, β, and γ. At the second rainbow ($q_{R2} = 0.29$ GeV/c), the points of stationary phase α and γ run together, and consequently the γ contribution will here be comparable to that coming from the trajectory denoted α.

Immediately beyond the second rainbow, at $q_R^{\mathrm{Coul}} = 0.33$ GeV/c, there is the (unphysical) Coulomb rainbow associated with the subtracted amplitude $F_C(q)$.

Downloaded from https://www.cambridge.org/core. UNIVERSIDAD AUTONOMA METROPOLITANA, on 16 Nov 2026 at 17:41:26, subject to the Cambridge Core terms of use, available at https://www.cambridge.org/core/terms. https://doi.org/10.1017/9781316219256.016

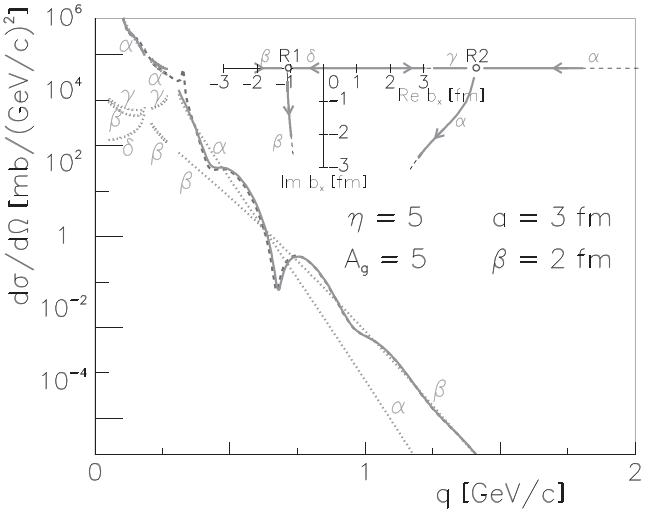


Figure 12.6 Differential cross section for the phase shift function Eq. (12.6). The inserts show the trajectories of stationary points for 0.1 GeV/c $\leq q \leq$ 5.0 GeV/c (dotted). The parts that correspond to 0.1 GeV/c $\leq q \leq$ 2.0 GeV/c are shown as solid curves (0.22 GeV/c $\leq q$ for α). The two open circles labeled "R1" and "R2" represent rainbow points. The cross sections contributed by the individual stationary points, α, β, γ, and δ, are shown as dotted curves. The solid curves give the resulting interference pattern, with gaps around $q_{R1} = 0.19$ GeV/c and $q_{R2} = 0.29$ GeV/c representing rainbow singularities.

Further out in momentum transfer, the contributions of α and β cross over in magnitude, leading to oscillations in the range of momentum transfer where they are comparable. Here, the stationary points α and β are both off the real axis. In contrast to the previous case of a repulsive nuclear interaction, in this case it is the β trajectory that dominates at large momentum transfers, not the "Coulomb" trajectory α.

12.2 Absorptive Gaussian Plus Coulomb

As an example of nuclear absorption plus Coulomb attraction, we now turn to the phase shift function Eq. (12.6) with $A_g = 5i$. The possible locations of stationary points are again easily determined from the map of real and imaginary parts of $X'(b_x)$ shown in Fig. 12.7, similar to those for the real cases, Figs. 12.3 and 12.4.

Again, there is a "Coulomb" trajectory (denoted α), which at small momentum transfers comes arbitrarily close to the real axis, but which for finite momentum transfers is always below the real axis. For the case of Coulomb repulsion considered here, it is located in the fourth quadrant of the complex b_x-plane. The cases of Coulomb repulsion and attraction are related by the symmetry Eq. (2.10).

The corresponding differential cross section is shown in Fig. 12.8. The result of a direct numerical integration is shown as a dashed curve, and is seen to yield a poor

Downloaded from https://www.cambridge.org/core. UNIVERSIDAD AUTONOMA METROPOLITANA, on 16 Nov 2026 at 17:41:26, subject to the Cambridge Core terms of use, available at https://www.cambridge.org/core/terms. https://doi.org/10.1017/9781316219256.016

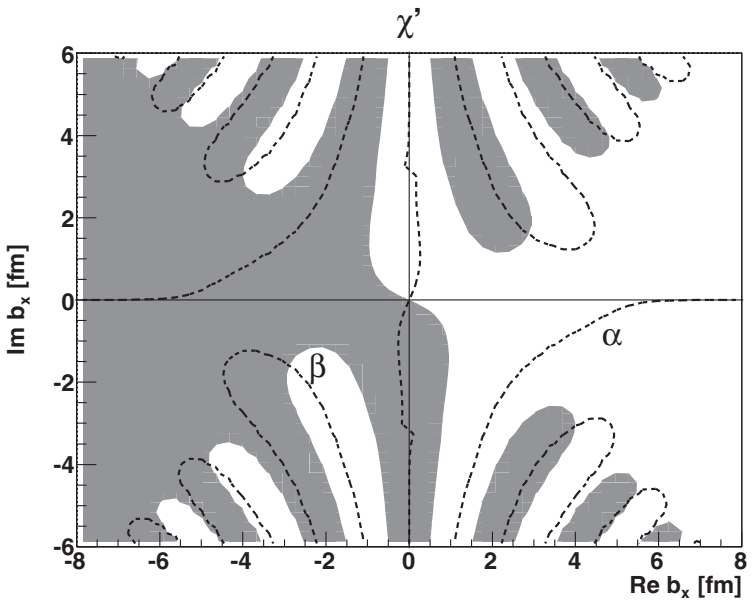


Figure 12.7 Regions of positive and negative values of $\mathrm{Re}\, X'(b_x)$, shown in the complex b_x-plane for $A_g = 5i$. The figure is analogous to Figs. 12.3 and 12.4, except that here the short-range nuclear interaction is purely absorptive.

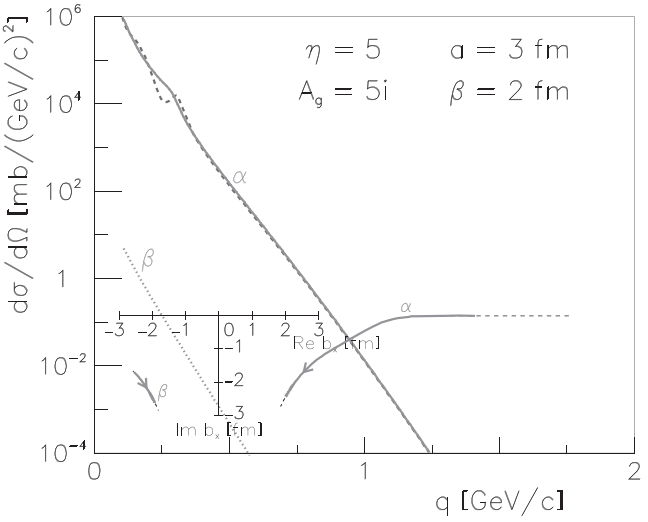


Figure 12.8 Differential cross section for the phase shift function Eq. (12.6). The inserts show the trajectories of stationary points for $0.15\ \mathrm{GeV/c} \le q \le 5.0\ \mathrm{GeV/c}$ (dotted). The parts that correspond to the cross section plots, $0.2\ \mathrm{GeV/c} \le q \le 3.0\ \mathrm{GeV/c}$ are shown as solid curves. The cross sections contributed by the individual stationary points, α and β are shown as dotted curves. The solid curve gives the resulting interference pattern.

Downloaded from https://www.cambridge.org/core. UNIVERSIDAD AUTONOMA METROPOLITANA, on 16 Nov 2026 at 17:41:26, subject to the Cambridge Core terms of use , available at https://www.cambridge.org/core/terms. https://doi.org/10.1017/9781316219256.016

result in the region of the Coulomb rainbow $q_R \simeq 0.33$ GeV/c, as discussed in the context of Eq. (12.5). As compared with the case of a purely absorptive Gaussian phase shift function, but no additional Coulomb interaction, studied in Section 7.3 (see, in particular, Fig. 7.6), the present phase shift function yields a very smooth cross section, with no oscillations. In terms of the trajectories of stationary points, this is caused by the α-trajectory being quite a bit closer to the real axis in the complex b_x-plane, due to the considerable strength of the Coulomb field. In fact, were the strength of the Coulomb field to be reduced, oscillations would gradually appear. At the same time, the envelope would become more steep. The case of a weaker Coulomb field will be illustrated in the next section.

12.3 "Fermi" Plus Coulomb

Consider next the phase shift function

$$X(b_x) = \frac{A_F}{1 + \exp[(b_x - c)/\beta]} + 2\eta \log\sqrt{a^2 + b_x^2}, \quad \mathrm{Re}\, b_x > 0,$$
$$X(-b_x) = X(b_x). \tag{12.10}$$

The short-range part of this has been studied in Section 8.4, under the title "Fermi" phase shift function. It has two shape parameters, c and β, for the radius and diffuseness of a "Fermi" distribution. The Coulomb part is the same as that considered previously in this chapter.

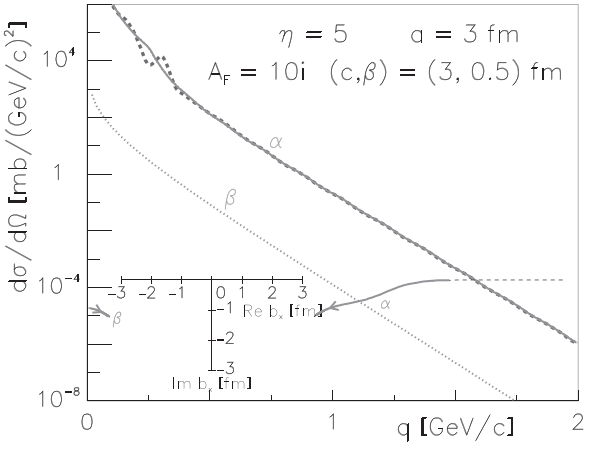


Figure 12.9 Differential cross section for the phase shift function Eq. (12.10). The inserts show the trajectories of stationary points for 0.15 GeV/c $\leq q \leq$ 4.0 GeV/c (dotted). The parts that correspond to 0.2 GeV/c $\leq q \leq$ 3.0 GeV/c are shown as solid curves. The cross sections contributed by the individual stationary points, α and β are shown as dotted curves. The solid curve gives the resulting interference pattern. The heavy dashed curve gives the result of a numerical integration.

Downloaded from https://www.cambridge.org/core. UNIVERSIDAD AUTONOMA METROPOLITANA, on 16 Nov 2026 at 17:41:26, subject to the Cambridge Core terms of use, available at https://www.cambridge.org/core/terms. https://doi.org/10.1017/9781316219256.016

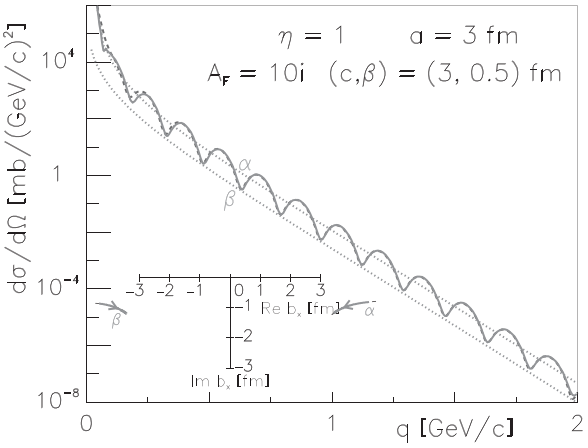


Figure 12.10 Differential cross section for the phase shift function Eq. (12.10). The inserts show the trajectories of stationary points for 0.15 GeV/c $\leq q \leq$ 4.0 GeV/c (dotted). The parts that correspond to 0.2 GeV/c $\leq q \leq$ 3.0 GeV/c are shown as solid curves. The cross sections contributed by the individual stationary points, α and β are shown as dotted curves. The solid curve gives the resulting interference pattern. The heavy dashed curve gives the result of a numerical integration.

We here focus on the case of an absorptive short-range interaction, with A_F pure imaginary. The shape parameters c and β are taken as 3 fm and 0.5 fm, respectively, values also studied in Section 8.4. For the strength of the Coulomb interaction, we consider two values, first a rather strong field, $\eta = 5$, in Fig. 12.9, and then a more moderate value, $\eta = 1$, in Fig. 12.10.

For the case of a stronger Coulomb field, the differential cross section is quite smooth. After a forward peak dominated by the Coulomb interaction, it has a smooth falloff, similar to that seen in Fig. 12.8 for the same strength of the Coulomb interaction. It is at all values of momentum transfer dominated by the contribution from the trajectory denoted α, which is the continuation of the Coulomb trajectory "down" into the absorptive regime, i.e., away from the real axis.

In Fig. 12.10 we study the case of a weaker Coulomb field, $\eta = 1$. This is roughly the magnitude relevant to proton scattering from lead. Compared with the case of a strong Coulomb field, the relative contributions from trajectories α and β are here more comparable, and, as a result, the differential cross section exhibits pronounced oscillations, similar to those seen in Section 8.4. The minima are however not zeros, since the amplitudes contributed by the two stationary points are somewhat different in magnitude, and therefore cannot completely cancel.

Downloaded from https://www.cambridge.org/core. UNIVERSIDAD AUTONOMA METROPOLITANA, on 16 Nov 2026 at 17:41:26, subject to the Cambridge Core terms of use , available at https://www.cambridge.org/core/terms. https://doi.org/10.1017/9781316219256.016